Investigation of Electron Delocalization and Ultrafast Studies of Ru^{II}/Os^{II} Dyads with Ethynyl/Butadiynyl-Bridged Polyphosphines

Dengfeng Xu, Jin Z. Zhang,† and Bo Hong*

Department of Chemistry, University of California, Irvine, California 92697-2025

Received: October 23, 2000; In Final Form: June 13, 2001

The redox characteristics, electronic absorption, steady-state emission, nanosecond laser flash photolysis, and a femtosecond laser spectroscopic study have been carried out for a series of monomeric, homobimetallic, and heterobimetallic complexes with $M(bpy)_2Cl$-based moieties (M = Ru^{II} and Os^{II}) and ethynyl- and butadiynyl-bridged polyphosphines, namely $Ph_2PC{\equiv}CPPh_2$ (**C_2P_2**) and $Ph_2PC{\equiv}CC{\equiv}CPPh_2$ (**C_4P_2**). These complexes were synthesized by reactions of the spacers with *cis*-$M(bpy)_2Cl_2$ or by coupling reaction between two $[Cl(bpy)_2M(Ph_2PC{\equiv}CH)](PF_6)$ (M = Ru^{II}, Os^{II}) molecules. Electronic communication through polyphosphine/polyyne spacers is found to decrease upon increase of the carbon chain length, and the comproportionation constant K_c was calculated as 14−18 for species with **C_2P_2** and ca. 4 for the ones with **C_4P_2**. In addition, fast intramolecular energy transfer from the Ru^{II}-based donor to the Os^{II}-based acceptor, with rate constant of $(2.4-2.5) \times 10^9$ s^{-1}, occurs within heterobimetallic complexes via a Dexter-type mechanism and an attenuation factor (β) of 0.02 $Å^{-1}$.

Introduction

Various low-dimensional multicomponent supramolecular systems have been designed and constructed owing to the longstanding interests in the mimetic modeling of natural photosynthesis and the study of directional electron/energy transfer as well as electronic interaction across bridging moieties.[1−9] Saturated and conjugated bridges have been applied, including flexible or rigid alkanes,[3] polyenes,[4] polyphenylene,[5] acetylenes,[6−8] and cumulenes,[9] in order to elucidate the parameters that govern the electron delocalization and electron/energy transfer processes. The tuning and optimization of such basic processes have attracted much attention due to the potential application of these supramolecular systems in optical and electronic devices as wires or switches and in artificial mimicry of light-energy conversion.

Among them, bimetallic one-dimensional rigid molecular complexes where metal centers are linked by the basic and fundamental class of unsaturated organic ligands, e.g., polyphenylenic (Ph_n) and cumulenic/acetylenic sp carbon chains (C_n), have provided the desired features such as rigidity, electronic conductivity, and coordination versatility.[5−9] We recently reported the preparation, electrochemical characteristics, and photophysical properties of a series of $Ru(bpy)_2$ and $Os(bpy)_2$ complexes with polyphosphines bearing short cumulenic bridging moieties, namely, 1,1′,3,3′-tetrakis(diphenylphosphino)-allene (**C_3P_4**) and 1,1′,4,4′-tetrakis(diphenylphosphino)cumulene (**C_4P_4**).[9] To compare the similarity and difference between the cumulenic and acetylenic sp carbon chains in redox-active and photoresponsive supramolecular systems, we now report the synthesis, characterization, redox chemistry, and ultrafast study of the systems **1**−**5** with $Ru(bpy)_2Cl$- and $Os(bpy)_2Cl$-based chromophores and ethynyl- and butadiynyl-bridged polyphosphine spacers $Ph_2P(C{\equiv}C)_nPPh_2$ (n = 1, **C_2P_2**, or 2, **C_4P_2**). Electronic absorption and cyclic and square-wave voltammetry (CV and SWV) are used to study the ground-state electronic and redox properties. Steady-state emission and ultrafast time-resolved emission and transient spectroscopic studies give us insights of the excited-state luminescence, decay kinetics, and energy transfer mechanism. Distance-dependent electronic communication and energy transfer via the Dexter mechanism are also discussed herein.

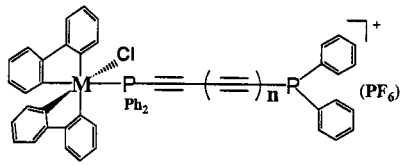

n = 0, M = Os, **1a**; Ru, **1b**
n = 1, M = Os, **2a**; Ru, **2b**

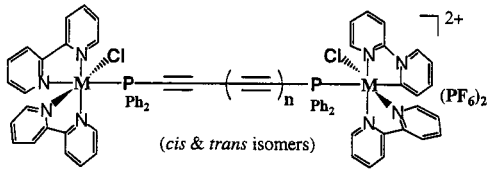

n = 0, M = M' = Os, **3a**; Ru, **3b**; M = Ru, M' = Os, **5a**
n = 1, M = M' = Os, **4a**; Ru, **4b**; M = Ru, M' = Os, **5b**

Results and Discussion

Synthetic Aspects. The monomeric and homobimetallic complexes **1a**−**4a** and **1b**−**4b** (synthesis of **1b** with ClO_4^- counteranion was previously reported using another method[10]) were synthesized using substitution reaction between *cis*-$(bpy)_2MCl_2{\cdot}2H_2O$ (M = Ru or Os) and **$C_{2n}P_2$** (n = 1 or 2) in different ratios: metal-to-ligand ratio of 1:2 to give predominantly monomeric complexes and 2.2:1 ratio to give homobimetallic ones (Scheme 1). However, no matter what ratios were used, the products always contained mixtures of the monomeric and homobimetallic complexes. Column chromatography (basic alumina) was required for purification, using different ratios of acetonitrile/toluene mixtures as eluants. Specifically, solvent

* To whom correspondence should be addressed.
† Present address: Department of Chemistry and Biochemistry, University of California, Santa Cruz, CA 95064.

10.1021/jp003907s CCC: $20.00
Published on Web 08/02/2001

SCHEME 1: Synthesis of Monomeric and Homobimetallic Species

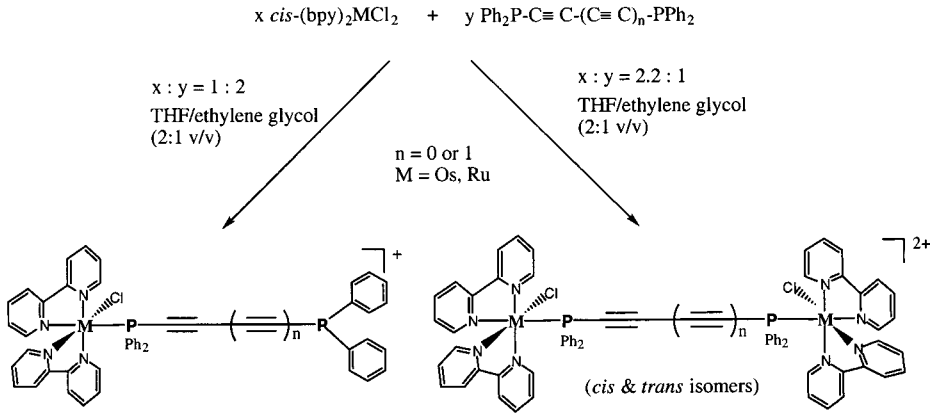

TABLE 1: $^{31}P\{^1H\}$ NMR and FAB/MS Data for 1a−5a and 1b−5b

complex	$^{31}P\{^1H\}$NMR (ppm)	FAB/MS: *m*/*z* (rel %), peak assgnt
1a	**−13.6 (Os^{II}−PPh_2)**	933 (80), $[M - PF_6]^+$
	−32.0 (free PPh_2)	539 (100), $[M - PF_6 - \mathbf{C_2P_2}]^+$
2a	**−11.5 (Os^{II}−PPh_2)**	957 (100), $[M - PF_6]^+$
	−30.6 (free PPh_2)	539 (90), $[M - PF_6 - \mathbf{C_4P_2}]^+$
1b	+33.3 (Ru^{II}−PPh_2)	843 (100), $[M - PF_6]^+$
	−32.0 (free PPh_2)	449 (98), $[M - PF_6 - \mathbf{C_2P_2}]^+$
2b	+35.9 (Ru^{II}−PPh_2)	867 (70), $[M - PF_6]^+$
	−30.6 (free PPh_2)	449 (100), $[M - PF_6 - \mathbf{C_4P_2}]^+$
3a	**−9.8**	1615 (50), $[M - PF_6]^+$
	−10.1	1470 (15), $[M - 2PF_6]^+$
		933 (100), $[M - 2PF_6 - Os(bpy)_2Cl]^+$
4a	**−10.7**	1639 (80), $[M - PF_6]^+$
	−10.9	1494 (10), $[M - 2PF_6]^+$
		957 (100), $[M - 2PF_6 - Os(bpy)_2Cl]^+$
3b	+37.7	1437 (50), $[M - PF_6]^+$
	+37.6	1292 (10), $[M - 2PF_6]^+$
		842 (100), $[M - 2PF_6 - Ru(bpy)_2Cl]^+$
4b	+36.7	1461 (70), $[M - PF_6]^+$
	+36.5	1316 (10), $[M - 2PF_6]^+$
		867 (100), $[M - 2PF_6 - Ru(bpy)_2Cl]^+$
5a	**−9.5, −9.7 (Os^{II}−PPh_2)**	1527 (25), $[M - PF_6]^+$
	+37.4, +37.2 (Ru^{II}−PPh_2)	1381 (10), $[M - 2PF_6]^+$
		933 (100), $[M - 2PF_6 - Ru(bpy)_2Cl]^+$
5b	**−10.6, −10.8 (Os^{II}−PPh_2)**	1551 (35), $[M - PF_6]^+$
	+36.5, +36.4 (Ru^{II}−PPh_2)	1405 (10), $[M - 2PF_6]^+$
		957 (100), $[M - 2PF_6 - Ru(bpy)_2Cl]^+$

mixture of acetonitrile/toluene (1:2, v/v) gave monomeric complexes, and 2:1 (v/v) gave homobimetallic species.

Heterobimetallic complexes (**5a**,**b**) were prepared from the further reaction of the Os^{II} monomeric complexes **1a** and **2a** with *cis*-$Ru(bpy)_2Cl_2 \cdot 2H_2O$. Theoretically it would be the same product starting from the Ru^{II} monomeric complexes **1b** or **2b** and *cis*-$Os(bpy)_2Cl_2 \cdot 2H_2O$. However, the former route provided higher reaction yields. It was found that the Ru^{II} center was more reactive toward phosphines than the Os^{II} ones, and more stringent conditions were required to form the more inert Os^{II} adducts.[1,9]

An alternative synthetic route, the coupling reaction, was also investigated to give bimetallic complexes with longer chain lengths (Scheme 2).[6] A 2 equiv amounts of the monomeric complexes $[Cl(bpy)_2M(Ph_2PC{\equiv}CH)](PF_6)$ (M = Ru, **6a,** or Os, **6b)** were coupled together in acetone solution to form **4a,b**, using CuCl/TMEDA as catalysis and O_2 as oxidant.[6c] Although the yield of the coupling reaction (40−51%) is not as high as the above substitution reactions (79−85%) for **4a,b**, it does provide additional means in the synthesis of rigid rodlike complexes with longer acetylenic chains.

Characterization. All complexes are characterized with $^{31}P\{^1H\}$ NMR, fast atom bombardment mass spectral analysis (FAB/MS), and elemental analysis (EA), Table 1. Monomeric complexes **1a** and **2a** and **1b** and **2b** exhibit two peaks in the $^{31}P\{^1H\}$ NMR spectra: a more positive one for M−PPh_2 (−11.5 to −13.6 ppm for M = Os and +33.3 to +35.9 ppm for M = Ru) and the more negative one for the free phosphine (−32.0 ppm for $\mathbf{C_2P_2}$ and −30.6 ppm for $\mathbf{C_4P_2}$). Because of the possible formation of isomers with cis and trans structures, each of the

SCHEME 2: Synthesis of Homobimetallic Species with a Coupling Reaction

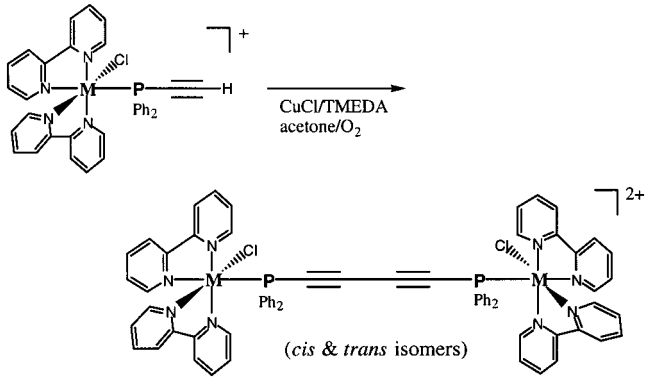

TABLE 2: Electrochemical Data for 1a−5a and 1b−5b

complex	$E_{1/2}$, V (ΔE_p) $Os^{II/III}$	$Ru^{II/III}$	$E_{1/2}$, V (ΔE_p) 1st $bpy^{0/-}$ redn	$E_{1/2}$, V (ΔE_p) 2nd $bpy^{0/-}$ redn
1a	+0.645 (1e⁻, 59)		−1.414 (1e⁻, 73)	−1.621 (1e⁻, 75)
2a	+0.666 (1e⁻, 67)		−1.429 (1e⁻, 66)	−1.654 (1e⁻, 60)
1b		+1.020 (1e⁻, 70)	−1.428 (1e⁻, 76)	−1.634 (1e⁻, 70)
2b		+1.044 (1e⁻, 79)	−1.471 (1e⁻, 70)	−1.705 (1e⁻, 66)
3a	+0.709 (1e⁻)[a]		−1.422 (2e⁻, 96)	−1.643 (2e⁻, 92)
	+0.635 (1e⁻)[a]			
4a	+0.705 (2e⁻, 99)		−1.448 (2e⁻, 86)	−1.664 (2e⁻, 80)
3b		+1.105 (1e⁻)[a]	−1.418 (2e⁻, 95)	−1.635 (2e⁻, 96)
		+1.037 (1e⁻)[a]		
4b		+1.058 (2e⁻, 100)	−1.478 (2e⁻, 85)	−1.717 (2e⁻, 88)
5a	+0.681 (1e⁻, 65)	+1.101 (1e⁻, 63)	−1.414 (2e⁻, 137)	−1.648 (2e⁻, 145)
5b	+0.671 (1e⁻, 65)	+1.057 (1e⁻, 62)	−1.457 (2e⁻, 110)	−1.710 (2e⁻, 140)
$Ru(bpy)_3(PF_6)_2$[14]	+1.29		−1.33	
$Os(bpy)_3(PF_6)_2$[13]		+0.81	−1.29	

[a] Data measured using square-wave voltammetry (SWV).

homobimetallic complexes **3a** (−9.8, −10.1 ppm), **4a** (−10.7, −10.9 ppm), **3b** (+37.7, +37.6 ppm), and **4b** (+36.7, +36.5 ppm) has two peaks. Each of the heterobimetallic complex **5a,b** has four peaks also due to the presence of the cis and trans isomers: two for $Ru-PPh_2$ (+36.4 to +37.4 ppm) and two for $Os-PPh_2$ (−10.8 to −9.5 ppm).

As a relatively soft ionization technique, FAB/MS is another excellent method for characterization. All the new complexes were ionized to give $[M - nPF_6]^+$ fragments ($n = 1$ or 2) in the higher molecular weight region, leaving the inner sphere of those compounds intact. Further loss of $\mathbf{C_{2n}P_2}$ ($n = 1$ or 2) from the monometallic complexes or loss of $M(bpy)_2Cl$ (M = Ru or Os) from the homo- and heterobimetallic species was also observed, Table 1.

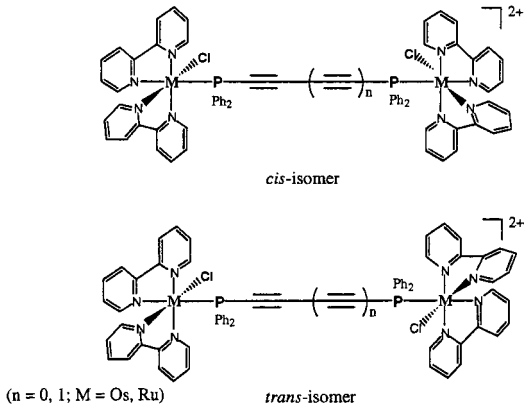

Electrochemistry. Cyclic voltammetry (CV) and square-wave voltammetry (SWV) were used to study the electrochemical behavior and possible electron delocalization. The metal-based oxidation and ligand-based reduction potentials are listed in Table 2, and Figure 1 compares the oxidation potentials of a series of Os^{II} mono- and bimetallic complexes.

Previously Ru^{II} center was reported to exhibit more positive oxidation potential than the Os^{II} one.[1] The $Os^{II/III}$ redox couple in **1a** or **2a** gives one reversible wave (1 e^- process) at $E_{1/2}$ = +0.645 and +0.666 V, while Ru^{II} complexes **1b** and **2b** give peaks at +1.020 and +1.044 V, respectively. The reversibility as used here implied that the i_p^a/i_p^c ratio was found to be approximately unity. Interestingly, complexes with $\mathbf{C_4P_2}$ exhibit slightly more positive potentials (~20 mV) when compared with the corresponding complexes with $\mathbf{C_2P_2}$, which suggests that $\mathbf{C_4P_2}$ is a stronger π acceptor than $\mathbf{C_2P_2}$ and renders the metal center harder to be oxidized.

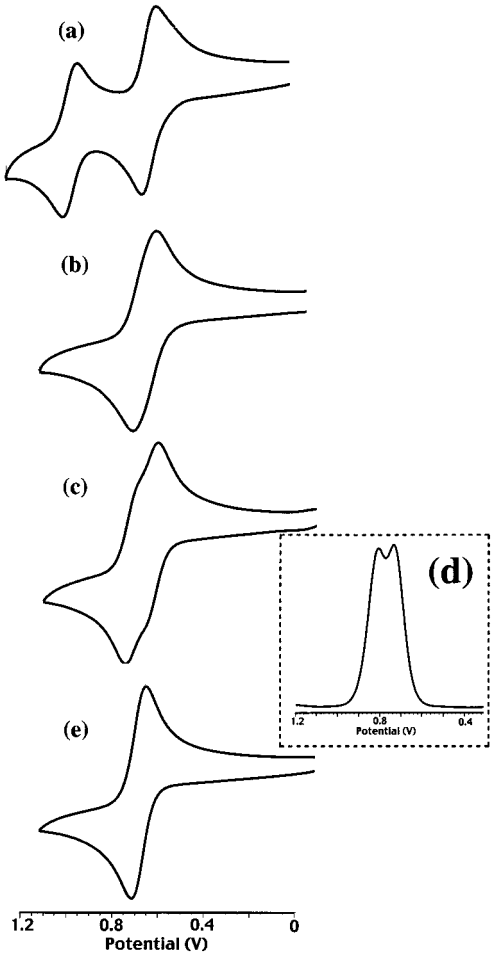

Figure 1. Metal-based oxidation wave in the CV of $[Cl(bpy)_2Ru(\mathbf{C_2P_2})Os(bpy)_2Cl](PF_6)_2$ (**5a)** (a), $[Cl(bpy)_2Os(\mathbf{C_4P_2})Os(bpy)_2Cl](PF_6)_2$ (**4a)** (b), $[Cl(bpy)_2Os(\mathbf{C_2P_2})Os(bpy)_2Cl](PF_6)_2$ (**3a)** (c), and $[(bpy)_2Os(\mathbf{C_2P_2})Cl](PF_6)$ (**1a)** (e) and SWV of $[Cl(bpy)_2Os(\mathbf{C_2P_2})Os(bpy)_2Cl](PF_6)_2$ (**3a)** (d).

Each of the homobimetallic complexes **3a**, **4a**, **3b,** and **4b** displayed two closely overlapping one-electron waves in the positive region. When SWV was employed, peak separations of 74 and 68 mV were observed for **3a** (Figure 1d) and **3b**, respectively. However, the peak separation was too small to be detected in the CV diagrams of homobimetallic **4a,b**. The observed peak separation in **3a,b** is ascribed to the consecutive oxidations of the two terminal metal units (eq 1), when a substantial amount of electronic delocalization exists across the

TABLE 3: Photophysical Data for 1a−5a and 1b−5b

complex	λ_{abs}, nm (ϵ, cm^{-1} M^{-1})	λ_{em},[a] nm (±5%)	$10^4\Phi$[a] (±10%)	τ_{em}, ns (±5%)[a]	$\eta_{isc}k_r$[b] (s^{-1})	k_{nr}[c] (s^{-1})
1a	291 (46 855) 442 (8080) 600 (2580)	540	1.1	11	1.0×10^4	9.1×10^7
2a	291 (43 425) 442 (7830) 595 (2360)	535	2.9	14	2.1×10^4	7.1×10^7
1b	291 (38 190) 441 (5950)	515	1.3	12	1.1×10^4	8.3×10^7
2b	291 (39 320) 432 (6080)	510	14	18	7.8×10^4	5.6×10^7
3a	293 (82 310) 436 (14 450) 595 (4220)	545	1.2	12	1.0×10^4	8.3×10^7
4a	291 (84 240) 438 (15 035) 595 (4070)	540	1.9	13	1.5×10^4	7.7×10^7
3b	291 (57 345) 434 (8520)	515	1.3	12	1.1×10^4	8.3×10^7
4b	291 (65 400) 432 (10 690)	510	9.5	15	6.3×10^4	6.7×10^7
5a	291 (70 160) 435 (11 580) 570 (2230)	545	1.2	0.38 (Ru^{II})[d] 11 (Os^{II})	1.1×10^4 (Os^{II})	2.6×10^9 (Ru^{II}) 9.1×10^7 (Os^{II})
5b	291 (70 890) 440 (12 790) 580 (2460)	540	2.8	0.40 (Ru^{II})[d] 14 (Os^{II})	2.0×10^4 (Os^{II})	2.5×10^9 (Ru^{II}) 7.1×10^7 (Os^{II})
$Ru(bpy)_3(PF_6)_2$[14a]	452	620	620	855	7.7×10^4	4.8×10^5
$Os(bpy)_3(PF_6)_2$[13b]	640	746	50	60	8.3×10^4	1.66×10^7

[a] $\lambda_{ex} = 470$ nm in CH_3CN. [b] $\eta_{isc}k_r = \Phi/\tau_{em}$. In 5a,**b**, only the longer lifetime is used in the calculation. [c] $k_{nr} = 1/\tau_{em} - \Phi/\tau_{em}$ (assuming $\eta_{isc} = 1$[14]). [d] $\lambda_{ex} = 390$ nm in CH_3CN.

central spacer $\mathbf{C_2P_2}$. Due to the electronic communication across the spacer, the second redox potential ($E_2°$) is expected to be more positive than the first one ($E_1°$), and the amount of peak separation can be used to probe the degree of such electronic communication between the two redox-active termini. This is manifested in the magnitude of the comproportionation constant K_c (eq 2), and K_c values have been found to range from 4 in the uncoupled Robin and Day class I system to 10^{13} in the strongly coupled class III system.[11d] Here, $M^{II}M^{II}$ represents the homobimetallic complexes, $M^{II}M^{III}$ and $M^{III}M^{III}$ are the oxidized species, and $E_1°$ and $E_2°$ (in mV) can be estimated from the metal oxidation potentials using SWV or CV.[11] Using eq 2, the comproportionation constants K_c for **3a,b** were estimated to be 14−18. For **4a,b**, K_c is ca. 4. (The peak separation in **4a,b** is ca. 34 mV, estimated from the difference of peak separation in **5a,b.** This is about 34 mV smaller than the peak separation within **3a,b**). On the basis of the different K_c values of these complexes, the electronic interaction was found to decrease, as expected, when the sp carbon atom number increases from 2 to 4 in the spacer unit.

$$M^{II}M^{II} \underset{e^-}{\overset{E_1°}{\rightleftharpoons}} M^{III}M^{II} \underset{e^-}{\overset{E_2°}{\rightleftharpoons}} M^{III}M^{III} \quad (1)$$

$$K_c = [M^{II}M^{III}]^2/[M^{II}M^{II}][M^{III}M^{III}] = \exp[(E_2° - E_1°)/25.69] \quad (2)$$

Previously, polyphosphines with cumulenic bridges, namely, $(Ph_2P)_2C{=}C{=}C(PPh_2)_2$ ($\mathbf{C_3P_4}$) and $(Ph_2P)_2C{=}C{=}C{=}C(PPh_2)_2$ ($\mathbf{C_4P_4}$) were also used by our group to study the electronic communication between the two terminal Os^{II} or Ru^{II} centers.[9] The complexes with longer $\mathbf{C_4P_4}$ were found to have much stronger electronic interaction ($K_c = 1.3 \times 10^7 - 4.5 \times 10^{10}$) than the corresponding complexes with $\mathbf{C_3P_4}$ (no significant redox peak separation was observed). This was caused by the fact that each odd carbon will rotate the pπ orbitals 90°, while the chain with even number of carbon atoms remains conjugated. However, the current systems with acetylenic C_2 and C_4 units have the coplanar dπ orbitals and, hence, the electronic communication is dominated by the distance between the two metal termini.

Heterobimetallic complexes **5a,b** exhibited two one-electron processes in the positive region, one corresponding to the $Os^{II/III}$ redox couple (+0.671 or +0.681 V) and the other corresponding to the $Ru^{II/III}$ pair (+1.057 or +1.101 V). This assignment is based on the observed redox potentials of the monometallic complexes **1a, 2a, 1b,** and **2b**. The larger peak separation between the $Os^{II/III}$ and $Ru^{II/III}$ redox potentials in **5a** (420 mV) than **5b** (386 mV) also suggests that $\mathbf{C_2P_2}$ is more conductive than $\mathbf{C_4P_2}$, giving rise to an increase in the electronic communication between the two metal termini. Hence, the conductivity order of $\mathbf{C_{2n}P_2}$ ($n = 1, 2$) and $\mathbf{C_nP_4}$ ($n = 3, 4$) is $\mathbf{C_4P_4} > \mathbf{C_2P_2} > \mathbf{C_4P_2} \approx \mathbf{C_3P_4}$, on the basis of the observed electrochemical data and calculated K_c values.

Furthermore, all complexes exhibit two ligand-based reduction peaks corresponding to the two $bpy^{0/-}$ redox couples,[12] both being quasi-reversible in the range of −1.414 to −1.478 V and −1.621 to −1.717 V, Table 2. For the monometallic complexes **1a, 2a, 1b,** and **2b**, each peak is an one-electron process. However, for bimetallic species **3a**−**5a** and **3b**−**5b**, each redox wave is a two-electron process, corresponding to two overlapping one-electron processes from the two equivalent bpy ligands on both metal centers.

Ground-State Electronic Absorption. All complexes were found to have strong absorption peaks at 291−293 nm (ϵ = 38 190−84 240 cm^{-1} M^{-1}) and 432−442 nm (ϵ = 5950−15 035 cm^{-1} M^{-1}; Table 3). The higher energy peak is assigned as a ligand-based $\pi \rightarrow \pi^*$ absorption. The lower energy band accounts for the ^{1}MLCT band, with M as a metal d_π orbital and L as a π^* orbital of bpy.[1] In addition, an Os^{II}-centered

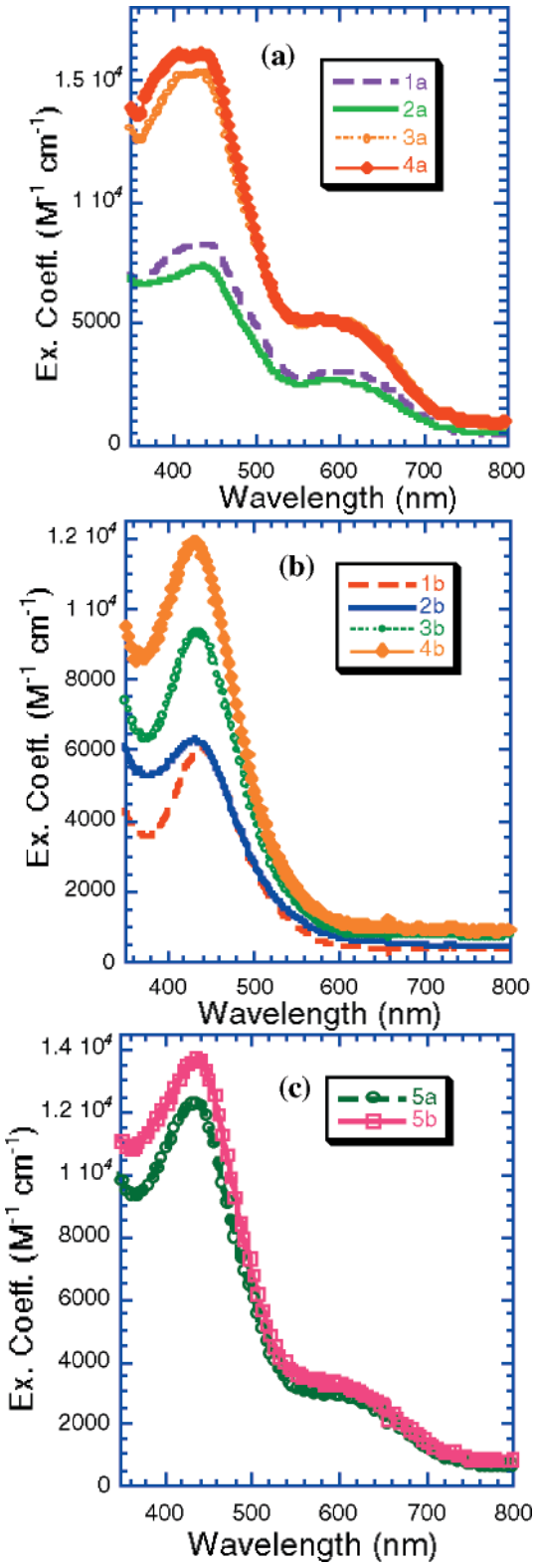

Figure 2. Comparison of electronic absorption spectra of **1a**−**4a** (a), **1b**−**4b** (b), and **5a,b** (c).

^{3}MLCT absorption was also observed at 570−600 nm (ϵ = 2360−4220 cm^{-1} M^{-1}) while Ru^{II} complexes do not exhibit a significant ^{3}MLCT band due to the lower spin−orbit coupling in Ru^{II} than in Os^{II}.[13]

Figure 2 displays the absorption spectra within 350−800 nm for all complexes. Several interesting features emerge when we compare them together. (a) The homobimetallic complexes **3a, 4a, 3b,** and **4b** give extinction coefficients nearly double that

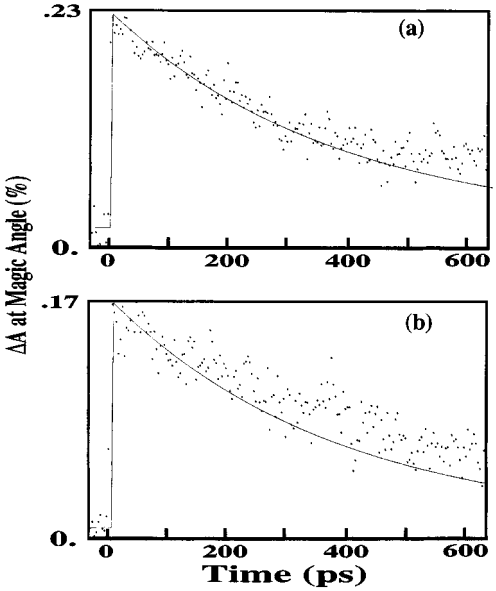

Figure 3. Transient time profiles of **5a,b** (λ_{ex} = 390 nm) in CH_3CN at 25 °C, following excitation at 390 nm, probed at wavelength 780 nm: (a) $[Cl(bpy)_2Ru(\mathbf{C_2P_2})Os(bpy)_2Cl](PF_6)_2$ (**5a**); (b) $[Cl(bpy)_2Ru(\mathbf{C_4P_2})Os(bpy)_2Cl](PF_6)_2$ (**5b**).

of the corresponding monomeric complexes **1a, 2a, 1b,** and **2b**, representative of a chromophore summation effect. (b) Os^{II} complexes have stronger MLCT absorption band when compared with the corresponding Ru^{II} complexes. (c) When compared with ^{1}MLCT bands of complexes $M(bpy)_3(PF_6)_2$[13] (M = Ru, λ_{MLCT} = 452 nm; M = Os, λ_{MLCT} = 640 nm), all the new compounds with $\mathbf{C_{2n}P_2}$ (n = 1, 2) have blue-shifted ^{1}MLCT absorption bands, which may be caused by the fact that $\mathbf{C_{2n}P_2}$ (n = 1, 2) are stronger π acceptors than the bpy ligand.

Emission, Lifetime, and Quantum Yield. Steady-state emissions of Ru^{II} monomeric and homobimetallic complexes were observed at 510−515 nm, while emissions of the corresponding Os^{II} complexes have maxima within 535−545 nm (Table 3). However, heterobimetallic complexes exhibit only one peak at 540−545 nm (from Os^{II} excited state) due to energy transfer from the Ru^{II} donor to Os^{II} acceptor as discussed later.

Time-resolved emission studies of all complexes have been carried out at room temperature in spectrophotometric grade acetonitrile. The emission decay traces of all complexes, except **5a,b**, fit to single-exponential decay curves, giving excited-state lifetimes from 11 to 18 ns, Table 3. Such short lifetimes from the emitting excited states may be ascribed to the possible mixing between the emitting excited state with the nonemissive ^{3}MC state in both Os^{II} and Ru^{II} complexes.[5b,13] The mixed-metal complexes **5a,b** have two lifetimes, with the shorter one (0.38−0.40 ns) corresponding to the quenched donor excited state and the longer one (11−14 ns) to the acceptor excited state. While the longer lifetimes were determined from the time-resolved emission measurements using nanosecond laser flash photolysis, the shorter lifetimes of the energy donors (Ru^{II}-based) were measured with femtosecond laser spectroscopy. Figure 3 displays the decay traces of the transient signals upon excitation at 390 nm for **5a,b**.

The radiative decay rate constant k_r and nonradiative decay rate constant k_{nr} for the emitting excited state can be calculated as $\eta_{isc}k_r = \Phi_{em}/\tau_{em}$ and $k_{nr} = 1/\tau_{em} - k_r = (1 - \Phi_{em}/\eta_{isc})/\tau_{em}$.[14] Here, Φ_{em} and τ_{em} are quantum yield and lifetime of emitting excited state and η_{isc} is the intersystem crossing efficiency. The values of all quantum yields (Φ_{em}) were measured to be (1.1−14) × 10^{-4}, as listed in Table 3. Since η_{isc} has not been

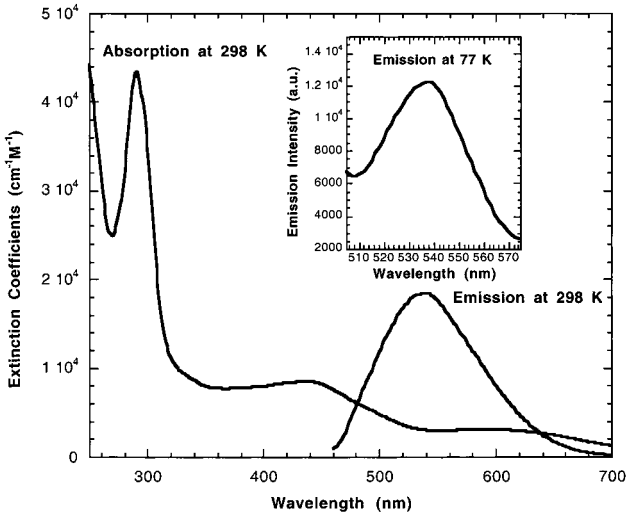

Figure 4. Comparison of the electronic absorption and emission (298 and 77 K) for $[(bpy)_2Os(\mathbf{C_4P_2})Cl](PF_6)$ (**2a**).

determined in our system, the $\eta_{isc}k_r$ values are calculated as $(1.0-7.8) \times 10^4$ s^{-1} and k_{nr} can be estimated, when assuming η_{isc} to be unity,[14] as $(5.6-9.1) \times 10^7$ s^{-1} for **1**−**5.** For the excited states of the Ru^{II}-based energy donors in the heterometallic systems **5a,b**, the k_{nr} values are found to be much higher, $(2.5-2.6) \times 10^{-9}$ s^{-1}. Such observed nonradiative decay rate constants are consistent with the observed low quantum yields and short lifetimes, suggesting that nonradiative decay path plays the dominating role in the excited-state decay kinetics in the current systems.

When we inspect the absorption and emission maxima of all new Os^{II} complexes, we noticed that the range of ^{3}MLCT absorption band (570−600 nm) is actually lower in energy than the observed emission maxima (535−545 nm) of the corresponding complexes, Table 3. The observed emission maxima of the Ru^{II} complexes are further blue-shifted to 510−515 nm. Previously, the analogous monomeric complexes $[(bpy)_2Ru(P)Cl](PF_6)$ (P = PPh_3, PPh_2Me) had no reported emission from the ^{3}MLCT state.[10] Hence, the observed emission in these new complexes with $\mathbf{C_{2}}_{n}\mathbf{P_2}$ (n = 1, 2) spacers cannot be simply attributed to the conventional ^{3}MLCT state (M → bpy, M = Ru or Os). Possible alternative excited states may exist. The polyphosphine/polyyne spacers and the polypyridyl auxiliary ligands used in this study most likely possess low-lying ring and polyyne π-antibonding orbitals that are capable of participation in the charge transfer interactions. Hence, the existence of a low-energy ligand-centered excited state is possible. Alternatively the ^{3}MLCT (M → phosphine spacer) state cannot be completely excluded as a possible emitting excited state.[12a] The following features have been observed regarding the excited-state characteristics. (a) As discussed above, the values of the radiative decay constant k_r are $(1.0-7.8) \times 10^4$ s^{-1} for all complexes reported here. These relatively low observed radiative decay constants may imply either rapid relaxation of the ^{1}MLCT state back to the ground state or formation of another excited state.[9b,12d] These values are also found to be sensitive to the polyphosphine spacer, with higher k_r values for complexes with $\mathbf{C_4P_2}$. (b) The emission measurements at 77 K in frozen MeCN matrix and at room temperature revealed little changes, and no significant blue shift was observed as expected for the metal-to-ligand charge-transfer bands.[12c] A comparison of the electronic absorption and emission at room temperature and 77 K for $[(bpy)_2Os(\mathbf{C_4P_2})Cl](PF_6)$ is shown in Figure 4. On the basis of these observations and data, we may assign the observed emission from the ligand-centered charge-transfer excited state. However, question arises regarding whether both ancillary bpy and central polyphosphine/polyyne spacer have been involved here. To resolve this, a calculation was done using the Spartan program. The distributions of electron densities on the HOMO and LUMO of the monometallic complexes **1b** and **2b** are included in Figure 5. Apparently in both complexes, the HOMO locates primarily on the C_2 or C_4 bridging unit of the central spacer and the LUMO locates primarily on one of the ancillary bpy ligand. This calculation suggests that the ligand-centered charge transfer may be ascribed as from polyphosphine/polyyne spacer → bpy.

Energy-Transfer Mechanism. Energy transfer from the Ru^{II}-based donor excited state to the Os^{II}-based acceptor within **5a,b** is evident for several reasons. (a) From steady-state emission study of both the monomeric and homobimetallic complexes it was found that the emitting excited states of Os^{II} units are lower in energy than those of the corresponding Ru^{II}-based ones. According to conventional assumptions,[15] the energetics or the driving force, $\Delta G°$, of energy transfer can be estimated as the difference between the spectroscopic energies of the donor and acceptor using homobimetallic species as model complexes. The calculated value is −1069 cm^{-1} (−0.13 eV) for **5a** and −1089 cm^{-1} (−0.14 eV) for **5b**. Hence, the energy transfer from the donor excited state to the acceptor one is thermodynamically favored. (b) The steady-state emission of the heterobimetallic complexes **5a,b** was dominated by the radiative decay from the acceptor. (c) Two lifetimes were found for **5a,b**. One is rather short (0.38−0.40 ns, Figure 3), corresponding to the quenched donor excited state. The other is longer (11−14 ns), corresponding to the acceptor excited state. For comparison, the lifetimes of Ru^{II}-based donor excited states in the mono- and homobimetallic species range from 12 to 18 ns, where no energy transfer is possible. Hence, the rate constant of energy transfer can be estimated as $k_{en} = 1/\tau - 1/\tau_m$,[15] where τ is the lifetime of the Ru^{II}-based energy donor in **5a,b** and τ_m is the lifetime of the homobimetallic model complexes **3b** and **4b**. The rate constants thus calculated are 2.5×10^9 s^{-1} for **5a** and 2.4×10^9 s^{-1} for **5b**.

Two possible mechanisms exist for the electronic energy transfer, namely, Förster- vs Dexter-type mechanism. For energy transfer via a Förster-type dipole−dipole (through space) mechanism, the appropriate spectroscopic overlap integral (J_F) can be expressed as eq 3:[1,7,9]

$$J_F = \frac{\int F(\nu)\epsilon(\nu)\nu^{-4}\,d\nu}{\int F(\nu)\,d\nu} \qquad (3)$$

Here $F(\nu)$ is the luminescence intensity at wavelength ν (in cm^{-1}) and $\epsilon(\nu)$ is the corresponding molar extinction coefficient (in M^{-1} cm^{-1}). The J_F value thus calculated is 2.7×10^{-14} and 2.9×10^{-14} cm^6 mol^{-1} (±10%) for the heterobimetallic complexes **5a,b**, respectively. The values obtained here are of comparable magnitude to the estimated overlap integrals previously reported for systems with rigid alkyne-[7] or phenylene-bridged[15b] Ru/Os complexes. The rate constant for triplet energy transfer via Förster mechanism can then be calculated using eq 4:[7]

$$k_F = \frac{8.8 \times 10^{-25} K^2 \Phi_L J_F}{n^4 \tau_L R^6} \qquad (4)$$

where K is the orientation factor relating to the alignment of transition dipoles on donor and acceptor ($K^2 = 0.67$[7b]), Φ_L and τ_L are the quantum yield and excited-state lifetime of the

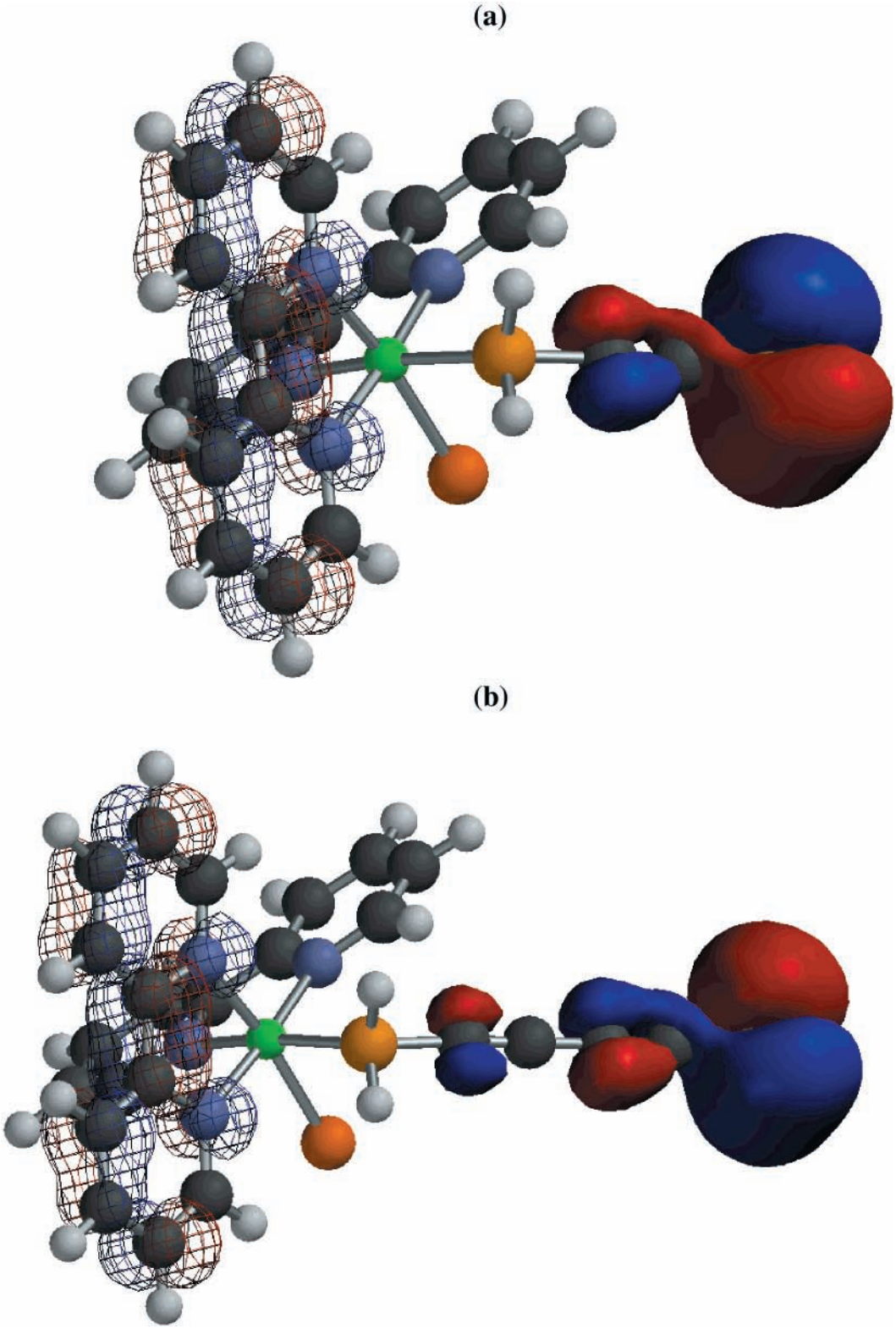

Figure 5. Spartan calculation of HOMO and LUMO in (a) **1b** and (b) **2b**.

appropriate model complex, and n is the refractive index of solvent acetonitrile. At 295 K the calculated k_F value is 1.9×10^8 s^{-1} over a metal-to-metal distance of $r = 8.0$ Å in **5a** with $\mathbf{C_2P_2}$ spacer and 3.2×10^7 s^{-1} over a metal-to-metal distance of 10.5 Å across $\mathbf{C_4P_2}$ spacer in **5b**. This calculated Förster energy transfer rate constant is much lower than the observed values of $(2.4-2.5) \times 10^9$ s^{-1}. Hence, an energy transfer exclusively through the Förster mechanism may not be suitable here.

For energy transfer occurring by way of a Dexter-type electron-exchange (i.e. through-bond) mechanism, the appropriate overlap integral (J_D) can be calculated from eq 5:[7d]

$$J_D = \frac{\int F(\nu)\epsilon(\nu)\,d\nu}{\int F(\nu)\,d\nu \int \epsilon(\nu)\,d\nu} \qquad (5)$$

The derived J_D values are 1.0×10^{-2} and 9.1×10^{-3} cm for

5a,b, respectively. The corresponding rate constant k_D can then be expressed in the following form:[7]

$$k_D = \frac{4\pi^2 H_{en}{}^2 J_D}{h} \quad (6)$$

where H_{en} is the electronic coupling matrix element for the electron exchange. When assuming that the energy transfer occurs exclusively via electron exchange and k_D has the values of the observed rate constant k_{en} of $(2.4-2.5) \times 10^9$ s^{-1}, then H_{en} will only need to have values of 0.46 cm^{-1} for **5a** and 0.47 cm^{-1} for **5b**. Such values correspond to a situation where the terminal Ru^{II} and Os^{II} centers have fairly weak interaction. The aforementioned electrochemical study has revealed a relatively weak redox interaction across $\mathbf{C_{2n}P_2}$ spacers ($n = 1$ or 2), with peak separation of ca. 34−74 mV. However, such redox separation is sufficient to drive the intramolecular energy transfer across the spacer unit. Hence, on the basis of all above calculations and observations, we may conclude that the Dexter-type energy transfer mechanism may dominate in the observed energy transfer process within the current heterobimetallic Ru/Os systems.

Dependence on Distance. In the study of intramolecular energy- or electron-transfer processes, another important issue is the distance dependence of the rate constant k_{en}. In the frame of superexchange mechanism, the energy transfer rate k_{en} falls off exponentially as in eq 7, with d_{MM} as the metal-to-metal distance.[7b,16]

On the basis of the observed k_{en} for **5a,b**, an attenuation factor β value of 0.02 $Å^{-1}$ was estimated for this system with polyphosphine/polyyne. Since only two points are used in the calculation of β value here, this can only serve as a crude estimation. When compared with the reported β values of other systems through alkenes ($\beta = 0.06$ $Å^{-1}$),[4] polypyridyl/polyynes ($\beta = 0.17$ $Å^{-1}$),[7] phenylene ($\beta = 0.4$ $Å^{-1}$),[1,17a] and fused alkanes ($\beta = 0.6-1.0$ $Å^{-1}$),[17b] we may conclude that the estimated β value of 0.02 $Å^{-1}$ in our system suggests that the polyphosphines spacers with short polyyne bridges can mediate sufficient electronic coupling to facilitate an efficient intramolecular energy transfer.

$$k_{en} \propto \exp(-\beta d_{MM}) \quad (7)$$

Experimental Section

General Procedures. All experiments described below were performed under a nitrogen atmosphere using standard glovebox and Schlenk techniques. Separations by column chromatography were performed in air and in the absence of light by using basic alumina (Brockman activity I, 60−325 mesh, from Fisher Scientific).

Materials. *cis*-$Os(bpy)_2Cl_2 \cdot 2H_2O$,[12] $Ph_2PC{\equiv}CH$ ($\mathbf{C_2PH}$)[18] and $PPh_2C{\equiv}CC{\equiv}CPPh_2$ ($\mathbf{C_4P_2}$)[19] were prepared according to the literature methods. $PPh_2C{\equiv}CPPh_2$ ($\mathbf{C_2P_2}$, Strem), CuCl (Aldrich, 99.9+%), TMEDA (Aldrich), *cis*-$Ru(bpy)_2Cl_2 \cdot 2H_2O$ (Strem), NH_4PF_6 (Aldrich), and KPF_6 (Aldrich) were purchased and used as received. Commercial grade solvents (acetonitrile, toluene, and diethyl ether) were dried over 4 Å molecular sieves prior to use. Spectrophotometric grade acetonitrile were purchased from Fisher and used without further purification. Tetrahydrofuran (THF) was distilled under nitrogen over sodium and benzophenone. Acetone was distilled under nitrogen over K_2CO_3. Ethylene glycol was dried over 4 Å molecular sieves for at least 24 h and deoxygenated with dry nitrogen for 20 min or longer prior to use.

Physical Measurements. $^{31}P\{^1H\}$ NMR spectra were obtained on Omega 500 MHz spectrometer, referenced to a solution of 85% H_3PO_4 in D_2O. Combustion analysis (C, H, N) was measured with a Carlo Erba Instruments Fisons elemental analyzer, and all data are included in the Supporting Information. Fast atom bombardment mass spectral analysis (FAB/MS) was recorded on a Micromass (Altrincham, U.K.) Autospec mass spectrometer at the UC, Irvine, CA, Mass Spectral Laboratory. Cerium ions at 25 kV were the bombarding species, and the matrix was *meta*-nitrobenzyl alcohol (mNBA).

Cyclic and square-wave voltammograms were recorded using a CHI 630 electrochemical analyzer. Typical experiments were run at a scan rate of 100 mV/s in spectrophotometric grade acetonitrile with 0.1 M tetrabutylammonium hexafluorophosphate as the electrolyte. A Ag/AgCl wire was used as a pseudoreference electrode, a platinum wire as the counter electrode, and a 1.0 mm platinum disk electrode as the working electrode. A ferrocene standard was used as the reference vs SCE.

Electronic absorption spectra were obtained on a Hewlett-Packard 8453 diode array spectrometer. Steady-state emission spectra were recorded on a Hitachi F-4500 fluorescence spectrometer. Quantum yields (QY) were measured relative to $Ru(bpy)_3(PF_6)_2$ (QY = 0.062[12,14] in CH_3CN), and all samples were treated with three freeze−pump−thaw cycles prior to the measurements.

Time-resolved emission of all complexes was carried out on a nanosecond flash photolysis unit. It is equipped with a Continuum Surelite II-10 Q-switched Nd:YAG laser and Surelite OPO (optical parametric oscillator) tunable visible source, a LeCroy 9350A oscilloscope, and a Spex 270 MIT-2x-FIX high-performance scanning and imaging spectrometer. All samples were dissolved in spectrophotometric grade acetonitrile and deoxygenated with dry N_2 for 30 min prior to the measurements.

For complexes **5a,b**, the transient time profiles were obtained using a pump−probe technique based on a regeneratively amplified, mode-locked femtosecond Ti−sapphire laser system. The details of the laser setup and the spectrometer have been described elsewhere.[20] All data were obtained with 390 nm excitation and probed at 780 nm, using spectrophotometric grade acetonitrile as solvent. Pulses of 40−100 fs with 5 nJ/pulse energy and 100 MHz repetition rate were generated by a mode-locked Ti−sapphire oscillator, which were then amplified using a Quantronix regenerative amplifier pumped with a Q-switched Nd:YLF laser. Final output pulses (150 fs, 350 μJ/pulse) at 780 nm were frequency doubled in a KDP crystal to generate a 390 nm pump beam with 30 μJ/pulse and 1 kHz repetition rate. The pump power was adjusted with neutral density filters so that no solvent signal was detected, and the observed signals were linear with pump power. The remaining fundamental was focused into a quartz crystal to generate a white light continuum. An interference band path filter (10 nm fwhm) was used to select the desired probe wavelength. The pump and probe beam were delayed in time using a translation stage, and the signal was detected by a silicon photodiode. The resulting signal was normalized to a reference signal from another photodiode monitoring the laser beam.

Molecular Orbital Calculation. Molecular orbital calculations were performed on Silicon Graphics Indigo2 XZ workstations, using Spartan V. 5.1.1-62 for IRIX developed by Wavefunction, Inc. The semiempirical PM3(tm) method with geometry optimization for transition metals was applied, which is related to Thiel's MNDO/d and describes each transition metal in terms of d-type, as well as s- and p-type, valence atomic

orbitals. All model structures without PF_6^- were minimized using the Spartan Builder. For computational purposes, all phenyl groups were replaced with protons. In the absence of Os^{II} parameters in the Spartan PM3(tm) program, only Ru^{II} model structures were used for calculations.

General Preparation of $[(bpy)_2M(C_2P_2)Cl](PF_6)$ (M = Os (1a), Ru (1b)), $[(bpy)_2M(C_4P_2)Cl](PF_6)$ (M = Os (2a), Ru (2b)), $[Cl(bpy)_2M(C_2P_2)M(bpy)_2Cl](PF_6)_2$ (M = Os (3a), Ru (3b)), and $[Cl(bpy)_2M(C_4P_2)M(bpy)_2Cl](PF_6)_2$ (M = Os (4a), Ru (4b)) from $M(bpy)_2Cl_2$ and $C_{2n}P_2$ (n = 1, 2). A solution of $C_{2n}P_2$ (n = 1 or 2) and *cis*-$(bpy)_2MCl_2 \cdot 2H_2O$ (M = Os or Ru) (2:1 ratio for mononuclear complexes **1a,b** and **2a,b**; 1:2.2 ratio for homobimetallic complexes **3a,b** and **4a,b**) in 30 mL of ethylene glycol/THF (1:2, v/v) was refluxed for 2 h. An excess amount of NH_4PF_6 (200−300 mg) was then added, and the mixture was refluxed for another 48 h to ensure the completion of reaction. The solution was cooled to room temperature, and THF was removed by rotary evaporation. The resulting ethylene glycol solution was added dropwise to a saturated solution of KPF_6 in 50 mL of H_2O under vigorous stirring. The precipitate was collected by vacuum filtration, washed with H_2O (3 × 10 mL) and diethyl ether (3 × 10 mL), and then dried in vacuo. The product was then purified by column chromatography using acetonitrile/toluene (1:2, v/v) as the eluant for the first fraction (**1a,b**, **2a,b**) and acetonitrile/toluene (2:1, v/v) as the eluant for the second fraction (**3a,b**, **4a,b**). Yields: **1a**, 61%; **1b**, 54%; **2a**, 65%; **2b**, 59%, **3a**, 80%; **3b**, 84%; **4a**, 79%; **4b**, 85%. Please refer to the Supporting Information for characterization data (elemental analysis, $^{31}P\{^1H\}$ NMR, and FAB/MS data).

General Preparation of $[Cl(bpy)_2Os(C_{2n}P_2)Ru(bpy)_2Cl](PF_6)_2$ (n = 1 (5a), 2 (5b)) from $M(bpy)_2Cl_2$ (M = Ru, Os) and $[(bpy)_2Os(C_{2n}P_2)Cl](PF_6)$ (n = 1 (1a), 2 (2a)). A solution of cis-$(bpy)_2RuCl_2 \cdot 2H_2O$ and $[(bpy)_2Os(C_{2n}P_2)Cl](PF_6)$ (n = 1 or 2; 1:1 ratio) in 30 mL of ethylene glycol/THF (1:2, v/v) was refluxed for 2 h. An excess amount of NH_4PF_6 (200−300 mg) was then added, and the mixture was refluxed for another 48 h. The solution was cooled to room temperature, and THF was removed by rotary evaporation. The resulting ethylene glycol solution was added dropwise to a saturated solution of KPF_6 in 50 mL of H_2O under vigorous stirring. The precipitate was collected by vacuum filtration, washed with H_2O (3 × 10 mL) and diethyl ether (3 × 10 mL), and then dried in vacuo. The solid was then purified by column chromatography. The second fraction was collected as the desired products using acetonitrile/toluene (2:1, v/v) as the eluant. Yield: **5a**, 77%; **5b**, 75%.

Preparation of $M(bpy)_2(C_2PH)Cl$ (M = Os (6a), Ru (6b)) from $M(bpy)_2Cl_2$ and $Ph_2PC{\equiv}CH$ (C_2PH). A solution of **C_2PH** and *cis*-$(bpy)_2MCl_2 \cdot 2H_2O$ (M = Os or Ru) (2:1 ratio) in 30 mL of ethylene glycol/THF (1:2, v/v) was refluxed for 2 h. An excess amount of NH_4PF_6 (200−300 mg) was added, and the mixture was heated under reflux for another 48 h. The solution was cooled to room temperature, and THF was removed using rotary evaporation. The resulting ethylene glycol solution was added dropwise to a saturated solution of KPF_6 in 50 mL of H_2O. The precipitate was collected by vacuum filtration, washed with H_2O (3 × 10 mL) and diethyl ether (3 × 10 mL), and then dried in vacuo. The product was then purified by column chromatography, and the first fraction was collected as the desired products using acetonitrile/toluene (1:2, v/v) as the eluant. Yield: **6a**, 98%; **6b**, 90%.

Alternative Preparation of $[Cl(bpy)_2M(C_4P_2)M(bpy)_2Cl](PF_6)_2$ (4a,b) from Coupling Reaction of $M(bpy)_2(C_2PH)Cl$ (6a,b) (M = Os, Ru). Hay catalyst was prepared by mixing CuCl (51 mg, 0.52 mmol) and TMEDA (41 μL) in 10 mL of acetone. The resulting mixture was stirred for 30 min. The blue supernatant was used in the subsequent reaction.[6c]

To a solution of **6a** or **6b** (ca. 0.1 mmol) in 20 mL of acetone, Hay catalyst was added and air was bubbled through. After the mixture was stirring for 2 h, solvent was removed using rotary evaporation. The resulting residue was dissolved in a minimum amount of CH_3CN and added dropwise to 30 mL of diethyl ether under vigorous stirring. The solid thus formed was collected by vacuum filtration and purified by column chromatography using acetonitrile/toluene (2:1, v/v) eluant. The second portion was collected as the desired product (yield 51% for **4a** and 40% for **4b**).

Acknowledgment. This work was supported by the University of California, Irvine, CA (UCI), and a National Science Foundation CAREER award (CHE-9733546). We thank Dr. John Greaves and staff (UCI Mass Spectral Laboratory) for their assistance in FAB/MS analysis.

Supporting Information Available: Characterization data (elemental analysis, $^{31}P\{^1H\}$ NMR, and FAB/MS data). This material is available free of charge via the Internet at http://pubs.acs.org.

References and Notes

(1) (a) Sauvage, J.-P.; Colin, J.-P.; Chambron, J.-C.; Guillercz, S.; Cudret, C.; Balzani, V.; Barigelletti, F.; De Cola, L.; Flamigni, L. *Chem. Rev.* **1994**, *94*, 993−1019. (b) Balzani, V.; Juris, A.; Venturi, M.; Campagna, S.; Serroni, S. *Chem. Rev.* **1996**, *96*, 759−833. (c) Balzani, V.; Scandola, F. *Supramolecular Photochemistry*; Horwood: Chichester, U.K., 1991.

(2) (a) Barbara, P. F.; Meyer, T. J.; Ratner, M. A. *J. Phys. Chem.* **1996**, *100*, 13148−13168. (b) Meyer, T. J. *Acc. Chem. Res.* **1989**, *22*, 163−170.

(3) (a) Padden-Row, A. D. *Acc. Chem. Res.* **1994**, *27*, 18−25. (b) Closs, G. L.; Miller, J. R. *Science* **1988**, *240*, 440−447. (c) Perkins, T. A.; Hauser, B. T.; Eyler, J. R.; Schanze, K. S. *J. Phys. Chem.* **1990**, *94*, 8745−8748. (d) Joran, A. D.; Leland, B. A.; Geller, G. G.; Hopfield, J. J.; Dervan, P. B. *J. Am. Chem. Soc.* **1984**, *106*, 6090−6092.

(4) (a) Baba, A. I.; Ensley, H. E.; Schmehl, R. H. *Inorg. Chem.* **1995**, *34*, 1198−1207. (b) Yonemoto, E. H.; Saupe, G. B.; Schmehl, R. S.; Hubig, S. M.; Riley, E. L.; Iverson, B. L.; Mallouk, T. E. *J. Am. Chem. Soc.* **1994**, *116*, 4786−4795. (c) Woitellier, S.; Launay, J. P.; Spangler, C. W. *Inorg. Chem.* **1989**, *28*, 758−762. (d) Benniston, A. C.; Goulle, V.; Harriman, A.; Lehn, J.-M.; Marczinke, B. *J. Phys. Chem.* **1994**, *98*, 7798−7804.

(5) (a) Wang, P.-W.; Fox, M. A. *Inorg. Chem.* **1995**, *34*, 36−41. (b) Paw, W.; Connick, W. B.; Eisenberg, R. *Inorg. Chem.* **1998**, *37*, 3919−3926.

(6) (a) Brady, M.; Weng, W.; Zhou, Y.; Seyler, J. W.; Amoroso, A. J.; Arif, A. M.; Böhme, A. M.; Frenking, G.; Gladysz, J. A. *J. Am. Chem. Soc.*, **1997**, *119*, 775−788. (b) Bartik, T.; Bartik, B.; Brady, M.; Dembinski, R.; Gladysz, J. A. *Angew. Chem., Int. Ed. Engl.* **1996**, *35*, 414−417. (c) Weng, W.; Bartik, T.; Brady, M.; Bartik, B.; Ramsden, J. A.; Arif, A. M.; Gladysz, J. A. *J. Am. Chem. Soc.* **1995**, *117*, 11922−11931.

(7) (a) Harriman, A.; Ziessel, R. *Chem. Commun.* **1996**, 1707−1716. (b) Grosshenny, V.; Harriman, A.; Ziessel, R. *Angew. Chem., Int. Ed. Engl.* **1995**, *34*, 1100−1102. (c) Grosshenny, V.; Harriman, A.; Remero, F. M.; Ziessel, R. *J. Phys. Chem.* **1996**, *100*, 0, 17472−17484. (d) Grosshenny, V.; Harriman, A.; Hissler, M.; Ziessel, R. *J. Chem. Soc., Faraday Trans.* **1996**, *92*, 2223−2238.

(8) (a) Lin, V. S.-Y.; DiMagno, S. G.; Therien, M. J. *Science* **1994**, *264*, 1105−1111. (b) Lin, V. S.-Y.; Therien, M. J. *Chem. Eur. J.* **1995**, *1*, 645−651.

(9) (a) Hong, B.; Ortega, J. V. *Angew. Chem., Int. Ed. Engl.* **1998**, *37*, 2131−2134. (b) Hong, B.; Woodcock, S. R.; Saito, S. K.; Ortega, J. V. *J. Chem. Soc., Dalton Trans.* **1998**, 2615−2623. (c) Ortega, J. V.; Hong, B.; Ghosal, S.; Hemminger, J. C.; Breedlove, B.; Kubiak, C. P. *Inorg. Chem.* **1999**, *38*, 5102−5112.

(10) Sullivan, B. P.; Salmon, D. J.; Meyer T. J. *Inorg. Chem.* **1978**, *17*, 3334−3341.

(11) (a) Richardson, D. E.; Taube, H. *Inorg. Chem.* **1981**, *20*, 1278−1285. (b) Richardson, D. E.; Taube, H. *Coord. Chem. Rev.* **1984**, *60*, 107−129. (c) Salaymeh, F.; Berhane, S.; Yusof, R.; de la Rosa, R.; Fung, E. Y.;

Matamoros, R.; Lau, K. M.; Zheng, Q.; Kober, E. M.; Curtis, J. C. *Inorg. Chem*. **1993**, *32*, 3895−3908. (d) Robin, M. B.; Day, P. *Adv. Inorg. Chem. Radiochem.* **1967**, *10*, 247−270.

(12) (a) Kober, E. M.; Caspar, J. V.; Sullivan, B. P.; Meyer, T. J. *Inorg. Chem.* **1988**, *27*, 4587- 4598. (b) Kober, E. M.; Marshall, J. L.; Dressick, W. J.; Sullivan, B. P.; Caspar, J. V.; Meyer, T. J. *Inorg. Chem.* **1985**, *24*, 2755−2763. (c) Lees, A. J. *Comments Inorg. Chem.* **1995**, *17*, 319−346. (d) Baba, A. I.; Ensley, H. E.; Schmehl, R. H. *Inorg. Chem.* **1995**, *34*, 4, 1198−1207.

(13) (a) Barigelletti, F.; Juris, A.; Balzani, V.; Belser, P.; von Zelewsky, A. *Inorg. Chem.* **1983**, *22*, 3335−3339. (b) Johnson, S. R.; Westmoreland, T. D.; Caspar, J. V.; Barqawi, K. R.; Meyer, T. J. *Inorg. Chem*. **1988**, *27*, 3195−3200.

(14) (a) Caspar, J. V.; Meyer, T. J. *J. Am. Chem. Soc.* **1983**, *105*, 5583−5590. (b) Caspar, J. V.; Sullivan, B. P.; Meyer, T. J. *Inorg. Chem.* **1984**, *23*, 2104−2109. (c) Demas, J. N.; Taylor, D. G. *Inorg. Chem.* **1979**, *18*, 3177−3179. (d) Mandal, K.; Pearson, T. D. L.; Krug, W. P.; Demas, J. N. *J. Am. Chem. Soc.* **1983**, *105*, 701−707.

(15) (a) Scandola, F.; Balzani, V. *J. Chem. Educ*. **1983**, *60*, 814−823. (b) Barigelletti, F.; Flamigni, L.; Balzani, V.; Colin, J.-P.; Sauvage, J.-P.; Sour, A.; Constable, E. C.; Thompson, A. M. W. C. *J. Am. Chem. Soc*. **1994**, *116*, 7692−7699.

(16) (a) McConnel, H. M. *J. Chem. Phys.* **1961**, *35*, 508−515. (b) Schlicke, B.; Belser, P.; De Cola, L.; Sabbioni, E.; Balzani, V. *J. Am. Chem. Soc.* **1999**, *121*, 4207−4214.

(17) (a) Osuka, A.; Maruyama, K.; mataga, N.; Asahi, T.; Yamazaki, I.; Tamai, N. *J. Am. Chem. Soc.* **1990**, *112*, 4958−4959. (b) Paddon-Row: M. N.; Shephard, M. J.; Jordon, K. D. *J. Phys. Chem*. **1993**, *97*, 1743−1745.

(18) Charrier, C.; Chodkiewicz, P.; Cadiot, W. *Mem. Soc. Chim.* **1965**, 1002−1011.

(19) Xu, D.; Hong, B. *Angew. Chem., Int. Ed. Engl.* **2000**, *39*, 1826−1829.

(20) (a) Zhang, J. Z.; O'Neil, R. H.; Roberti, T. W. *J. Phys. Chem.* **1994**, *98*, 3859−3864. (b) Howe, L.; Zhang, J. Z. *J. Phys. Chem.* **1997**, *101*, 3207−3213.